α-Radioimmunotherapy of Intraperitoneally Growing OVCAR-3 Tumors of Variable Dimensions: Outcome Related to Measured Tumor Size and Mean Absorbed Dose

Jörgen Elgqvist[1], Håkan Andersson[2], Tom Bäck[1], Ingela Claesson[2], Ragnar Hultborn[2], Holger Jensen[3], Bengt R. Johansson[4], Sture Lindegren[1], Marita Olsson[5], Stig Palm[1], Elisabet Warnhammar[2], and Lars Jacobsson[1]

[1]Department of Radiation Physics, The Sahlgrenska Academy at Göteborg University, Göteborg, Sweden; [2]Department of Oncology, The Sahlgrenska Academy at Göteborg University, Göteborg, Sweden; [3]PET and Cyclotron Unit, Rigshospitalet, Copenhagen, Denmark; [4]The Electron Microscopy Unit, Institute of Anatomy and Cell Biology, Göteborg University, Göteborg, Sweden; and [5]Bioinformatics Core Facility, Göteborg University, and Department of Mathematical Statistics, Chalmers University of Technology, Göteborg, Sweden

The purpose of this work was to (a) investigate the efficacy of radioimmunotherapy using ^{211}At-MX35 F(ab′)$_2$ or ^{211}At-Rituximab F(ab′)$_2$ (nonspecific antibody) against differently advanced ovarian cancer in mice; (b) image the tumor growth on the peritoneum; and (c) calculate the specific energy and mean absorbed dose to tumors and critical organs. **Methods:** Two experiments with 5-wk-old nude mice (n = 100 + 93), intraperitoneally inoculated with ~1 × 10^7 NIH:OVCAR-3 cells, were done. At either 1, 3, 4, 5, or 7 wk after inoculation animals were intraperitoneally treated with ~400 kBq ^{211}At-MX35 F(ab′)$_2$ (n = 50 + 45), ~400 kBq ^{211}At-Rituximab F(ab′)$_2$ (n = 25 + 24), or unlabeled Rituximab F(ab′)$_2$ (n = 25 + 24). At the time of treatment 29 animals were sacrificed and biopsies were taken for determination of tumor sizes using scanning electron microscopy (SEM). Eight weeks after each treatment the animals were sacrificed and the presence of macro- and microscopic tumors and ascites was determined. The specific energy and mean absorbed dose to tumors were calculated. The activity concentration was measured in critical organs and abdominal fluid. **Results:** When given treatment 1, 3, 4, 5, or 7 wk after cell inoculation the tumor-free fraction (TFF) was 95%, 68%, 58%, 47%, 26%, and 100%, 80%, 20%, 20%, and 0% when treated with ^{211}At-MX35 F(ab′)$_2$ or ^{211}At-Rituximab F(ab′)$_2$, respectively. The SEM images revealed maximum tumor radius of ~30 μm 1 wk after cell inoculation, increasing to ~340 μm at 7 wk. Specific energy to cell nuclei varied between 0 and ~540 Gy, depending on assumptions regarding activity distribution and tumor size. The mean absorbed dose to thyroid, kidneys, and bone marrow was ~35, ~4, and ~0.3 Gy, respectively. **Conclusion:** Treatment with ^{211}At-MX35 F(ab′)$_2$ or ^{211}At-Rituximab F(ab′)$_2$ resulted in a TFF of 95%−100% when the tumor radius was ≤30 μm. The TFF was decreased (TFF ≤ 20%) for ^{211}At-Rituximab F(ab′)$_2$ when the tumor radius exceeded the range of the α-particles. The specific antibody gave for these tumor sizes a significantly better TFF, explained by a high mean absorbed dose (>22 Gy) from the activity bound to the tumor surface and probably some contribution from penetrating activity.

Key Words: ovarian cancer; radioimmunotherapy; dosimetry; astatine; MX35

J Nucl Med 2006; 47:1342–1350

Ovarian cancer, one of the most common causes of death among gynecologic malignant disease in the Western world, is often lethal in spite of complete clinical remission after surgery and systemic chemotherapy for residual disease mainly localized on the peritoneal surfaces (*1*). Conventional paclitaxel/platinum-based chemotherapy is not specific to tumor cells and is often ineffective because of cellular resistance mechanisms (*2*). However, monoclonal antibodies (mAbs) have made targeted therapy possible, by mediating cytotoxicity either by direct immunotoxicity or by labeling mAbs with radionuclides (*3*).

Some studies have been performed on the radioimmunotherapeutic efficacy on ovarian cancer of β-emitters, mostly ^{90}Y and ^{131}I labeled to mAbs, in animals and humans (*4–14*). Because of the fact that the β-particles emitted from these radionuclides have too long a range for the treatment of microscopic tumors we believe it is of great interest to investigate the therapeutic efficacy of α-particle emitters labeled to mAbs when treating microscopic disease. In this study we used the α-particle emitter ^{211}At, with a half-life of 7.21 h, its α-particles having a mean range in tissue of ~62 μm and a mean linear energy transfer (LET) of ~111 keV/μm. The short range of the α-particles ensures a significant absorbed dose to small tumors or single cells (*15*). The high LET of the α-particles together with a high relative biological effectiveness (RBE), for ^{211}At on subcutaneous OVCAR-3 tumors in nude mice determined to 4.8 ± 0.7 (*16*), indicate

Received Dec. 20, 2005; revision accepted Mar. 6, 2006.
For correspondence or reprints contact: Jörgen Elgqvist, PhD, Department of Radiation Physics, The Sahlgrenska Academy at Göteborg University, SE-413 45 Göteborg, Sweden.
E-mail: jorgen.elgqvist@radfys.gu.se

that only a small number of ^{211}At atoms have to be targeted to a cell to get a high probability for sterilization. We have previously investigated the therapeutic efficacy using the intact IgG1 mAbs MOv18 and MX35 when treating mice with ovarian cancer at approximately 3 wk after cell inoculation (*17–20*). Those studies showed a good therapeutic effect with a tumor-free fraction (TFF) of ~60%. We also found indications that there was some therapeutic effect of nonspecific mAbs.

MATERIALS AND METHODS

Radionuclides

^{211}At was produced by the ^{209}Bi(α,2n)^{211}At reaction in a cyclotron (Scanditronix MC32 at the Positron Emission Tomography and Cyclotron Unit, Rigshospitalet, Copenhagen, Denmark) by irradiating a ^{209}Bi target with 28-MeV α-particles. The ^{211}At was isolated using a dry-distillation procedure (*21*). ^{125}I was obtained commercially (PerkinElmer Life and Analytic Sciences).

mAbs

MX35 is a murine IgG1-class mAb, developed and characterized at the Memorial Sloan-Kettering Cancer Center (MSKCC), New York, NY. MX35 is directed toward a cell-surface glycoprotein of ~95 kDa on OVCAR-3 cells (*22*) and is expressed strongly and homogeneously on ~90% of human epithelial ovarian cancers (*23*). A batch of MX35 F(ab′)$_2$, produced by Strategic BioSolutions for clinical use, was provided by MSKCC. Rituximab (Genentech, Inc.) is a chimeric human/mouse anti-CD20 IgG1-class mAb (*24*) and was chosen as a nonspecific mAb. The IgG1 Rituximab was fragmented using the ImmunPure F(ab′)$_2$ kit (Pierce Chemical Co.). The F(ab′)$_2$ fragments were subsequently additionally purified by size-exclusion chromatography on a Superdex 200 column (GE Healthcare).

Antibody Labeling

mAbs were labeled with ^{211}At using the labeling reagent *m*-MeATE (*N*-succinimidyl 3-(trimethylstannyl)benzoate) (*25*). ^{211}At, in 10 mmol/L NaOH, was added to a mixture of *m*-MeATE and *N*-iodosuccinimide in methanol:1% acetic acid. This solution was incubated for 10 min at room temperature and the labeling reaction was stopped by adding sodium ascorbate. The mAb, MX35 F(ab′)$_2$ or Rituximab F(ab′)$_2$, was added and conjugation was allowed to proceed for 20 min. The mAb fraction was isolated using a NAP-5 column (Amersham Biosciences), resulting in a specific activity of 136 ± 24 kBq/μg mAb—that is, 1 of ~1,200 mAbs labeled with an ^{211}At atom. The radiochemical yields were in the range of 30%−40% and the radiochemical purity was >95% as determined by methanol precipitation and gel-permeability chromatography.

^{125}I-Radioiodination of the mAbs was performed using basically the same conditions as those described, except that *N*-bromosuccinimide was used instead of *N*-iodosuccinimide as the oxidizing agent.

Cell Line

The cell line OVCAR-3 (NIH:OVCAR-3: National Institutes of Health ovarian cancer cell line 3) was used (*26*). The cell line was obtained from the American Type Culture Collection. The cells were cultured in T-75 culture flasks at 37°C in a humidified atmosphere of 95% O_2/5% CO_2 with RPMI 1640 cell culture medium supplemented with 10% fetal calf serum, 1% L-glutamine, and 1% penicillin–streptomycin.

Immunoreactivity of Antibodies

The immunoreactivity of the mAbs was analyzed by determination of the immunoreactive fraction, *r*. A fixed amount of MX35 F(ab′)$_2$ or Rituximab F(ab′)$_2$ (10 ng in 0.040 mL medium—i.e., 1.7 nmol/L) was added to single-cell suspensions of OVCAR-3 cells, in duplicate, to a final volume of 0.540 mL. The cells were suspended in cell culture medium at 6 different concentrations, ranging from 5 to 0.16 million/mL. After incubation with gentle agitation for 2 h at room temperature, the cells were centrifuged and rinsed twice in phosphate-buffered saline (PBS). Specific binding to the cells was determined by radioactivity measurements of the rinsed pellets in a NaI(Tl)-well detector (Wizard 1480; Wallac Oy.). The value of *r* was finally derived from a plot of total applied radioactivity divided by cell-bound radioactivity as a function of the inverse of the cell concentration (*27*). The maximum number of MX35 F(ab′)$_2$ bound per OVCAR-3 cell, B_{max}, and the association rate constant, k_{on} (i.e., the rate at which the mAbs are bound to the antigenic sites on the cell surface for a specific antigen concentration), were determined as previously described (*20*).

Scanning and Transmission Electron Microscopy

Specimens for ultrastructural analysis were obtained from mice anesthetized with Metofane (Mallinckrodt Veterinay Inc.). The thoracic cavity was exposed and the heart root was clamped to arrest blood flow, after which an intraperitoneal injection (5 mL) of a mixture of 2.5% glutaraldehyde, 2% paraformaldehyde, and 0.01% sodium azide in 0.05 mol/L sodium cacodylate (pH 7.2) was given. After 10 min of primary fixation, the abdominal cavity was exposed and specimens, including peritoneal lining, were harvested by dissection from various anatomic locations (ventral abdominal wall, diaphragm, liver, spleen, kidneys, ileum and jejunum [including mesenteries], and colon). Specimens were further fixed overnight in the aldehyde mixture. After rinsing in 0.15 mol/L cacodylate, specimens for scanning electron microscopy (SEM) were subjected to an OTOTO postfixation procedure (*28*). Dehydration followed in a series of ethanol, finally replaced by 2 changes of hexamethyldisalazane, which was allowed to evaporate under a fume hood. The dried specimens were mounted on aluminum stubs and were examined in a Zeiss 982 Gemini field emission scanning electron microscope after coating with palladium in an Emitech 550 sputter coater. Digital images were collected at a resolution of 1,024 × 1,024 pixels. Each specimen (~16 mm^2) was examined in the microscope.

Specimens intended for transmission electron microscopy (TEM) were postfixed for 2 h in 1% OsO_4 with 1% potassium ferrocyanide in 0.1 mol/L cacodylate. After rinsing in water they were stained en bloc with 0.5% uranyl acetate for 1 h followed by dehydration in ethanol and propylene oxide. The tissue blocks were infiltrated with epoxy resin (Agar 100) and cured by heating. Ultrathin sections were cut on a Reichert Ultracut 5E microtome fitted with a diamond knife at a thickness setting of 50–60 nm. Sections were contrasted with uranyl acetate and lead citrate before examination in a LEO 912AB Omega-transmission electron microscope. Digital images were collected with a MegaView III camera (Soft Imaging System).

Radiation Dosimetry

As the nucleus was considered to be the most radiation-sensitive part of the cell, the specific energy to tumor cell nuclei ($r_{nucleus} \approx 7.2$ μm, $m_{nucleus} \approx 1.6$ ng) in tumors on the peritoneum

was calculated for various tumor sizes and activity distributions. The cell packing ratio was assumed to be 1.0 in each tumor—that is, assuming no intercellular space. For spheric tumors with radii, r_{tumor}, equal to 30, 45, 95, 160, and 340 μm the number of cells, n_{cell}, was approximately 35, 120, 1,180, 5,620, and 53,920, and the corresponding tumor mass, m_{tumor}, was 0.1, 0.4, 3.6, 17.2, and 164.6 μg, respectively ($r_{cell} \approx 9.0$ μm). In the case of surface-distributed activity, a "cobble-stone" surface, where half of the mantle surface of the outermost cells is exposed, was assumed. The total number of antigenic sites in a whole tumor volume was then $B_{max} \times n_{cell}$, and the number of sites on the tumor surface was $2 \times B_{max} \times$ (sphere area/cell area), where B_{max} is the maximum number of mAbs able to bind to a tumor cell.

The cumulated activity on a tumor cell was calculated with an in-house developed compartmental model (*20*). Previously described software (*29*) was used for dosimetry in tumors. The software uses stopping power values of α-particles in liquid water (*30*) for Monte-Carlo–derived dosimetry and was designed to calculate the energy deposition and α-particle track length for each 0.01 μm in a defined target volume—here a 7.2-μm-radius sphere, simulating a single tumor cell nucleus embedded at various depths in the tumor.

Spheric tumors with r_{tumor} equal to 30, 45, 95, 160, and 340 μm were used. The calculations were set in cubic matrices with side lengths always larger than $2 \times r_{tumor}$ for bound activity and $2 \times r_{tumor} + s_{max}$ for unbound activity, where s_{max} is the maximum path length in liquid water of the 7.45-MeV α-particle from the decay of ^{211}Po (~71 μm). The target, the cell nucleus, remained at the center of the matrix to include the full range of those α-particles that could contribute to the number of events in the target. The software was run for 3,000 recorded α-particle events in each target, giving an error of $\sqrt{3,000}/3,000$—that is, 1.8%, according to Poisson statistics.

The mean specific energy at each target position was assigned the corresponding tumor shell. The mean absorbed dose (D) was calculated by averaging the mean specific energy over all shells. When relating the therapeutic outcome to the mean absorbed dose to the entire tumor, an index f was used at some mean absorbed dose values, indicating the fraction of unirradiated cells in the core of those tumors. This was done for tumors for which $r_{tumor} > s_{max}$.

The mean absorbed dose in the critical organs thyroid and kidneys was obtained by calculating the cumulated activities in each organ, based on the biokinetic data presented here. The mean absorbed dose to bone marrow was calculated according to our previously presented method (*31*).

Animals and Study Groups

Female nude BALB/c *nu/nu* mice (Charles River Laboratories International Inc.) were used ($n = 225$). The animals were housed at ~22°C and ~55% humidity with a light/dark cycle of 12 h. Two batches ($n = 100 + 93$) were then each divided into 15 groups and treated as shown in Table 1. Twenty and 12 nontumor–bearing animals were used to study the temporal activity concentration variation in the abdominal fluid and the biodistribution of ^{211}At-MX35 F(ab′)$_2$ after intraperitoneal injection, respectively. The experiments were approved by the Ethics Committee of Göteborg University, Sweden.

Procedures

At the age of 5 wk, 100 animals were inoculated intraperitoneally with ~1×10^7 OVCAR-3 cells suspended in 0.2 mL NaCl. Four weeks later this procedure was repeated for the second batch of animals ($n = 93$). At 1, 3, 4, 5, or 7 wk after cell inoculation, the animals were injected intraperitoneally with 387–419 kBq (in 1.0 mL PBS) ^{211}At-MX35 F(ab′)$_2$ ($n = 50 + 45$), 391–424 kBq ^{211}At-Rituximab F(ab′)$_2$ ($n = 25 + 24$), or unlabeled Rituximab F(ab′)$_2$ ($n = 25 + 24$), as indicated in Table 1. On each treatment occasion—that is, at 1, 3, 4, 5, or 7 wk after cell inoculation—animals were sacrificed from the groups given unlabeled Rituximab ($n = 29$) and biopsies were taken and prepared for SEM as described above, enabling estimation of tumor size.

Eight weeks after treatment the animals were sacrificed and dissected. The presence of macroscopic tumors and ascites was assessed by ocular inspection. Multiple biopsies were taken from the peritoneum (upper left quadrant of abdominal wall), diaphragm, spleen, and jejunum (including mesentery); fixed in formaldehyde and dehydrated with xylene; embedded in paraffin; cut into 4-μm-thick slices; and stained with eosin and hematoxylin for light microscopy. The presence of microscopic tumor growth was assessed with a magnification of up to ×40.

One group of nontumor–bearing animals ($n = 20$) was used to study the temporal variation in the activity concentration in the abdominal fluid after intraperitoneal injection of 1.0 mL ^{125}I-MX35 F(ab′)$_2$. The amount of injected activity was ~230 kBq. At 0.5, 1.0, 1.5, 4.0, and 7.5 h after injection, 4 animals were sacrificed by cervical dislocation. The abdominal cavity was exposed and a 10- or 20-μL capillary tube was used to collect samples of the abdominal fluid. All samples were weighed and the activity was measured in a NaI(Tl)-well detector.

Another group of nontumor–bearing animals ($n = 12$) was used for the study of the in vivo distribution of ^{211}At- and ^{125}I-MX35 F(ab′)$_2$. The amount of intraperitoneally coinjected activity was ~330 kBq ^{211}At-MX35 F(ab′)$_2$ and ~65 kBq ^{125}I-MX35 F(ab′)$_2$. At 1, 3, 6, and 19 h after injection 3 animals were sacrificed, and blood, spleen, throat (including thyroid), lungs, liver, stomach, small intestine, large intestine, kidneys, heart, fat (intraperitoneal), salivary glands, and muscle were collected. All samples were weighed and the activity was measured in a NaI(Tl)-well detector. ^{125}I-MX35 F(ab′)$_2$ was included to study potential differences of the in vivo stability of the radiopharmaceuticals.

Statistical Analysis

Logistic regression models were set up in SPSS software (SPSS Inc.) and used to evaluate the effects of type of treatment and time of treatment on the probability of the animals remaining tumor free. The best-fitting model included not only both covariates "treatment" (^{211}At-MX35 F(ab′)$_2$ or ^{211}At-Rituximab F(ab′)$_2$), and "time" (1, 3, 4, 5, or 7 wk after cell inoculation) but also their interaction: "treatment × time". The fact that the inclusion of the interaction term gave a significantly better fit ($P = 0.007$) of the model to the dataset means that the 2 treatments acted differently at different times of treatment—that is, the odds ratios for treatment with ^{211}At-MX35 F(ab′)$_2$ versus treatment with ^{211}At-Rituximab F(ab′)$_2$ was not constant for different times of treatment.

RESULTS

The immunoreactive fraction, r, of MX35 F(ab′)$_2$ and Rituximab F(ab′)$_2$ for OVCAR-3 cells was 0.96 ± 0.03 and 0.02 ± 0.01 (mean ± SEM), respectively. The association rate constant, k_{on}, and the maximum number of mAbs that can bind

TABLE 1
Study Groups and Therapeutic Results (n = 164)

Group	n	Type of treatment		Time of treatment (no. of weeks after cell inoculation)	Macroscopic tumors	Mean tumor weight (mg)		Microscopic tumors	Ascites	TFF* (%)
						Total group	Animals with macroscopic tumors			
1	19	^{211}At-MX35 F(ab′)$_2$	~400† kBq in PBS	1	1/19	3.7	70.3	1/19	0/19	95
2	19	^{211}At-MX35 F(ab′)$_2$	~400† kBq in PBS	3	2/19	5.7	54.2	6/19	4/19	68
3	19	^{211}At-MX35 F(ab′)$_2$	~400† kBq in PBS	4	7/19	6.2	16.8	8/19	9/19	58
4	19	^{211}At-MX35 F(ab′)$_2$	~400† kBq in PBS	5	10/19	68.0	129.2	10/19	10/19	47
5	19	^{211}At-MX35 F(ab′)$_2$	~400† kBq in PBS	7	14/19	117.5	160.0	14/19	14/19	26
6	10	^{211}At-Rituximab F(ab′)$_2$	~400‡ kBq in PBS	1	0/10	0.0	0.0	0/10	0/10	100
7	10	^{211}At-Rituximab F(ab′)$_2$	~400‡ kBq in PBS	3	1/10	5.5	55.0	2/10	1/10	80
8	10	^{211}At-Rituximab F(ab′)$_2$	~400‡ kBq in PBS	4	8/10	6.4	8.0	8/10	8/10	20
9	10	^{211}At-Rituximab F(ab′)$_2$	~400‡ kBq in PBS	5	7/10	65.9	94.1	8/10	6/10	20
10	9	^{211}At-Rituximab F(ab′)$_2$	~400‡ kBq in PBS	7	6/9	174.3	261.4	9/9	9/9	0
11	4	Unconjugated Rituximab F(ab′)$_2$	in PBS	1	4/4	270.5	270.5	4/4	4/4	0
12	4	Unconjugated Rituximab F(ab′)$_2$	in PBS	3	4/4	97.0	97.0	4/4	4/4	0
13	4	Unconjugated Rituximab F(ab′)$_2$	in PBS	4	4/4	70.0	70.0	4/4	4/4	0
14	4	Unconjugated Rituximab F(ab′)$_2$	in PBS	5	4/4	121.6	121.6	4/4	4/4	0
15	4	Unconjugated Rituximab F(ab′)$_2$	in PBS	7	4/4	487.9	487.9	4/4	4/4	0

*TFF = % with no macro- or microscopic tumors and no ascites.
†Injected activity was 387–419 kBq.
‡Injected activity was 391–424 kBq.
PBS = phosphate-buffered saline.
The presence of macroscopic tumors and ascites was assessed by careful ocular inspection during dissection 8 wk after administration of the different regimens. Microscopic tumor growth was assessed in paraffin-embedded biopsies, stained with eosin–hematoxylin, and light microscopy at 40× magnification.

to an OVCAR-3 cell, B_{max}, was $6.6. \times 10^4 \pm 0.4 \times 10^4$ [mol/L]$^{-1} \times$ [s]$^{-1}$ and $1.2 \times 10^6 \pm 2.3 \times 10^5$ (mean ± SEM), respectively.

Therapeutic Outcome

The results from the 2 batches were very similar and were therefore pooled (Table 1). Mice treated with ~400 kBq ^{211}At-MX35 F(ab′)$_2$ (groups 1–5) showed a high TFF (95%) when the treatment was given 1 wk after cell inoculation. As the time of treatment was postponed, an increasing number of animals developed macro- and microscopic tumors and ascites, resulting in TFFs of 68%, 58%, 47%, and 26% for treatment given 3, 4, 5, or 7 wk after cell inoculation, respectively. For mice given ~400 kBq ^{211}At-Rituximab F(ab′)$_2$ (groups 6–10), a greater decrease in TFF was seen at delayed treatment. The TFFs were 100%, 80%, 20%, 20%, and 0% when treatment was given 1, 3, 4, 5, or 7 wk after cell inoculation, respectively. The efficacy of ^{211}At-MX35 F(ab′)$_2$ was better, compared with ^{211}At-Rituximab F(ab′)$_2$, when treatment was given later, indicating the importance of cellular binding of the mAb as the tumor size increase. The mean tumor mass expressed as the total tumor weight of the group as well as per animal with macroscopic growth is given in Table 1.

The calculated probability of being tumor free was high, ~0.94 and ~0.74, for both treatment regimens (^{211}At-MX35 F(ab′)$_2$ or ^{211}At-Rituximab F(ab′)$_2$) provided that treatment was given early—that is, 1 or 3 wk after cell inoculation, respectively. However, for treatment 5 or 7 wk after cell inoculation, the probability of an animal being tumor free was low (~0.09 and ~0.01) when given ^{211}At-Rituximab F(ab′)$_2$, whereas it was higher when given ^{211}At-MX35 F(ab′)$_2$ (~0.48 and ~0.23). Table 2 shows that for treatment 1 or 3 wk after cell inoculation the odds of being tumor free were not significantly different for the 2 regimens, whereas from 4 wk after cell inoculation and onward the odds ratios increased exponentially in favor of treatment with ^{211}At-MX35 F(ab′)$_2$ ($P < 0.05$).

Tumor Growth

Figure 1 shows a SEM image of a single OVCAR-3 microvilli-covered cell loosely adhered to the peritoneum (Fig. 1A). Maximum tumor sizes found at the different times of treatment are shown in Figs. 1B–1F. Tumor cells adjacent to the mesothelium were often flattened and could penetrate under the mesothelial cell layer. Figure 2 shows a TEM image of an OVCAR-3 cell adhered to the mesothelial cell layer of the peritoneum. According to estimates made from SEM and TEM images, the cell and cell nucleus were determined to be 2 concentric spheres with radii of 9.0 and 7.2 μm, respectively.

Radiation Dosimetry

An ~27% decrease was observed of the activity concentration during the first 4 h after injection (Fig. 3). Thereafter, the major part of the fluid had been reabsorbed, making further measurements difficult. An exponential curve was fitted to the data, enabling calculation of the concentration later than 4 h after injection. The ~27% decrease in activity concentration caused an ~7% decrease in the cumulated cell-bound activity and, therefore, was included in the radiation dosimetry.

The results from the study of the biodistribution of ^{211}At- and ^{125}I-MX35 F(ab′)$_2$ are presented in Table 3. There is an increased uptake in the thyroid, lungs, stomach, kidneys, and salivary glands of ^{211}At-MX35 F(ab′)$_2$ compared with ^{125}I-MX35 F(ab′)$_2$. The mean absorbed dose to thyroid, kidneys, and bone marrow owing to ^{211}At uptake was ~35, ~4, and ~0.3 Gy, respectively.

The specific energy originating from activity bound on the tumor cells, and that originating from unbound activity in the abdominal fluid, is presented in Figure 4. In the case in which the ^{211}At-MX35 F(ab′)$_2$ was assumed to be homogeneously distributed throughout the whole tumor, the specific energy to cell nuclei varied between ~150 and ~530 Gy for 400 kBq ^{211}At-MX35 F(ab′)$_2$. For the tumor-surface-distributed ^{211}At-MX35 F(ab′)$_2$, the specific energy to cell nuclei never fell below ~65 Gy for $r_{tumor} = 45$ μm. The minimum value for the unbound contribution for this tumor never fell below ~11 Gy. For tumors with radii greater than s_{max} (i.e., tumors with $r_{tumor} = 95$, 160, or 340 μm) the specific energy was zero to cell nuclei in the core of the tumor.

Figure 5 illustrates the TFF as a function of the mean absorbed dose in tumors for specific and nonspecific mAbs for the different irradiation geometries. The relatively low value of TFF for the surface-distributed irradiation (▲) of the tumor with $r_{tumor} = 340$ μm, despite the high mean absorbed dose, is explained by the large fraction of unirradiated cell nuclei ($f = 0.495$) in the core of such tumors—that is, $D_{0.495} \approx 22$ Gy.

TABLE 2
Estimated Odds Ratios (OR) for Treatment with ^{211}At-MX35 F(ab′)$_2$ vs. ^{211}At-Rituximab F(ab′)$_2$ Controlling for Time of Treatment

Parameter	1 wk	3 wk	4 wk	5 wk	7 wk
OR	0.11	0.94	2.79	8.25	72.32
95% CI	0.005, 2.24	0.26, 3.39	1.02, 7.61	1.70, 39.95	2.34, 2,237.06

CI = confidence interval.

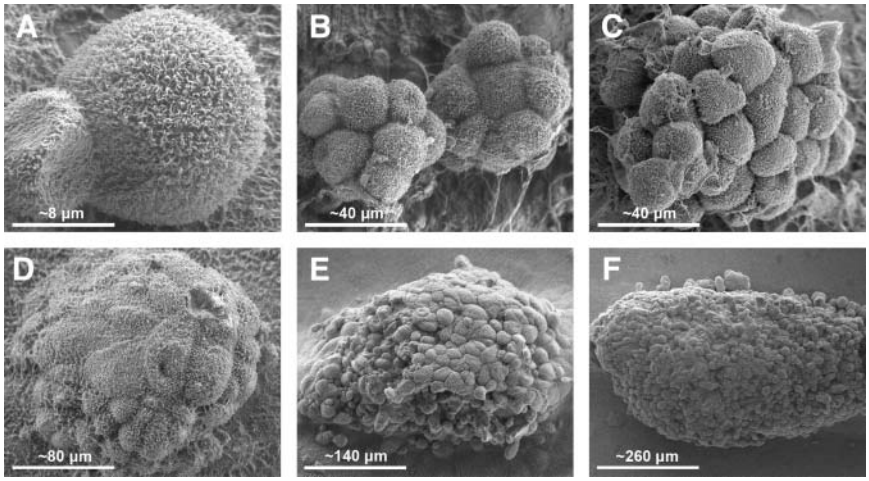

FIGURE 1. SEM images show single OVCAR-3 cell (A) and maximum-sized tumors on peritoneum at treatment times at 1 (B), 3 (C), 4 (D), 5 (E), and 7 (F) wk after cell inoculation. Specimens shown were taken from upper left quadrant of abdominal wall. Tumors in B–F represent examples of the largest tumor found in each study group, respectively. Tumor cells adhered to peritoneum and subsequently developed tumors, giving impression of an increasing adherence to, and occasionally penetration under, mesothelial cell layer.

DISCUSSION

Some studies of the therapeutic efficacy of ^{90}Y-, ^{131}I-, ^{177}Lu-, and ^{186}Re-labeled mAbs for ovarian cancer have been performed in both animals and humans (*4–14*). One study has used the α-emitter ^{212}Pb (*32*).

The β-particles emitted from radionuclides mentioned above have a range that is too long (~1–11 mm) to effectively irradiate microscopic tumors and also have a half-life that is too long to be optimal for intraperitoneal use. ^{211}At, with a mean particle range in soft tissue of ~62 μm and a half-life of 7.21 h, therefore seems to be ideal once the disease has been macroscopically removed, but with microscopic residual disease restricted to the peritoneal surfaces.

We have previously investigated the therapeutic efficacy of ^{211}At-mAbs when treatment was given intraperitoneally 2–3 wk after inoculation of OVCAR-3 cells (*17–20*). In studies with 400 kBq ^{211}At-MOv18, the TFF was 70%–90%. With the same activity of ^{211}At-MX35 the TFF was 80% for treatment given 3 wk after inoculation. The results of these studies showed some effect of a nonspecific mAb, TFF = 25%. To clarify these findings the present study was initiated to explain the therapy outcome from a dosimetric point of view and the dependence on tumor size. As an earlier study had shown that MX35 had no antineoplastic effect (*20*), we included only cold Rituximab F(ab′)$_2$ as control in the present study. An activity level of 400 kBq was chosen on the basis of experience from these previous studies as well as on a study of the myelotoxicity (*31*). A mean absorbed dose of 4 Gy to the kidneys due to

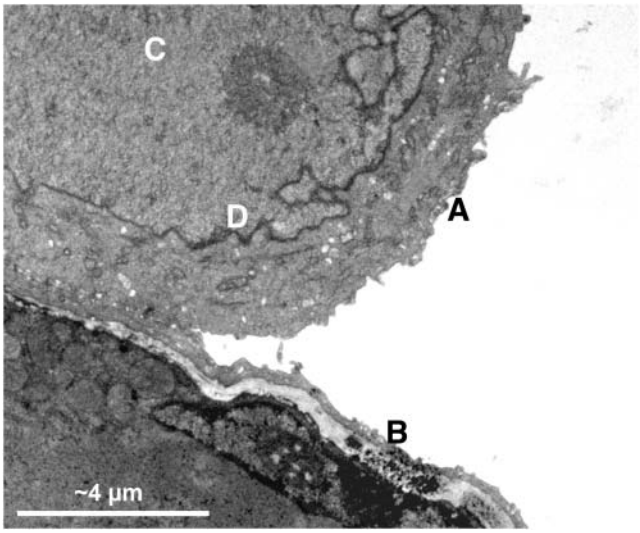

FIGURE 2. TEM image shows single spherically shaped OVCAR-3 cell covered with microvilli (A) that adhered to mesothelial cell layer (B) on peritoneum. The relatively large nucleus ($r_{nucleus} \approx 0.8 \times r_{cell}$) of the cell can also be seen (C), together with its envelope (D). The specimen shown was taken from upper left quadrant of abdominal wall.

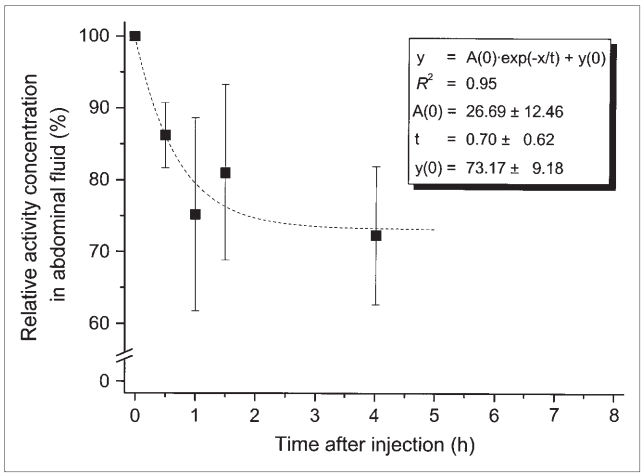

FIGURE 3. Relative abdominal activity concentration (■, $n = 4$ at each time) at 0.5, 1.0, 1.5, and 4.0 h after intraperitoneal injection of ~230 kBq ^{125}I-MX35 F(ab′)$_2$ in 1 mL (i.e., ~0.23 kBq/μL). An exponential curve was fitted (- - -) to the data points. At 7.5 h after injection, amount of abdominal fluid was not sufficient for activity measurements. Values are mean ± SEM.

TABLE 3
Percentage of Injected Activity per Gram (%IA/g) for Intraperitoneally Injected ^{211}At- and ^{125}I-MX35 F(ab′)$_2$ (n = 12)

	1 h		3 h		6 h		19 h	
Biodistribution	^{211}At-MX35	^{125}I-MX35	^{211}At-MX35	^{125}I-MX35	^{211}At-MX35	^{125}I-MX35	^{211}At-MX35	^{125}I-MX35
Blood (cardiac)	13.65 ± 1.48	11.68 ± 1.04	9.94 ± 1.04	8.64 ± 0.56	13.80 ± 1.34	10.44 ± 0.80	3.56 ± 0.71	2.07 ± 0.46
Fat (i.p.)	3.39 ± 0.15	2.99 ± 0.15	6.02 ± 0.58	5.55 ± 0.32	9.43 ± 0.60	7.06 ± 0.58	1.76 ± 0.34	0.46 ± 0.12
Heart	1.13 ± 0.49	0.89 ± 0.42	2.69 ± 0.31	1.72 ± 0.15	4.20 ± 0.36	2.39 ± 0.18	1.83 ± 0.26	0.42 ± 0.09
Kidneys	3.73 ± 1.04	4.22 ± 1.32	11.89 ± 2.06	12.98 ± 1.74	23.33 ± 3.16	20.69 ± 2.26	4.40 ± 0.76	2.53 ± 0.57
Large intestine	0.64 ± 0.10	0.59 ± 0.07	1.75 ± 0.10	1.29 ± 0.12	3.45 ± 0.09	2.16 ± 0.06	1.54 ± 0.16	0.39 ± 0.08
Liver	1.54 ± 0.50	1.31 ± 0.44	2.29 ± 0.31	1.82 ± 0.19	2.98 ± 0.27	2.14 ± 0.17	1.19 ± 0.14	0.42 ± 0.08
Lungs	2.39 ± 0.50	1.53 ± 0.43	5.74 ± 0.87	3.15 ± 0.65	8.99 ± 0.74	3.79 ± 0.30	6.22 ± 0.62	0.79 ± 0.15
Muscle	0.69 ± 0.27	0.68 ± 0.27	1.19 ± 0.07	0.98 ± 0.10	1.62 ± 0.27	1.06 ± 0.25	0.60 ± 0.11	0.21 ± 0.04
Salivary glands	1.14 ± 0.32	0.57 ± 0.17	2.72 ± 0.50	1.09 ± 0.15	6.17 ± 0.23	1.88 ± 0.21	6.07 ± 1.24	0.44 ± 0.09
Small intestine	1.14 ± 0.30	0.91 ± 0.26	2.06 ± 0.29	1.58 ± 0.16	3.48 ± 0.17	2.09 ± 0.06	1.52 ± 0.23	0.29 ± 0.05
Spleen	1.14 ± 0.12	0.71 ± 0.13	2.80 ± 0.30	1.35 ± 0.17	4.35 ± 0.09	1.56 ± 0.02	2.93 ± 0.33	0.33 ± 0.06
Stomach	2.64 ± 0.28	1.39 ± 0.15	5.93 ± 0.69	2.35 ± 0.16	8.34 ± 0.69	2.35 ± 0.20	7.36 ± 2.39	0.32 ± 0.06
Thyroid*	10.47 ± 4.36	6.55 ± 3.13	91.35 ± 34.47	20.40 ± 1.20	104.51 ± 9.39	29.45 ± 2.33	178.13 ± 32.03	7.76 ± 1.37

*Activity concentration (ac) in thyroid was calculated considering weight (w) of and activity (a) in throat specimen and a standard weight (sw) of thyroid of 3 mg for nude BALB/c *nu/nu* mice. Throat was assumed to contain samples of both muscle and thyroid. Consequently, the calculation was done as follows: $\text{Thyroid}_{ac} = (\text{Throat}_a - (\text{Throat}_w - \text{Thyroid}_{sw}) \times \text{Muscle}_{ac})/\text{Thyroid}_{sw}$.

i.p. = intraperitoneal.

Values are corrected for radioactive decay and are presented as means ± SEM.

α-particle irradiation cannot be disregarded. Therefore, studies on potential renal toxicity are now being performed.

The rationale for selecting MX35 F(ab′)$_2$ in this study was that (a) we have received an approval by the Swedish Medical Products Agency for carrying out a phase I trial, for females with recurrent ovarian cancer, with this fragmented mAb; (b) we believe that the diffusion into tumors using a F(ab′)$_2$ fragment is higher than compared with whole IgG1; and (c) if repeated treatment (i.e., fractionated RIT) will be considered for humans we believe that the immunogenicity of the F(ab′)$_2$ fragment is lower than that of whole IgG1, reducing the risk for a human antimurine antibody response.

^{211}At decays with a half-life of 7.21 h in 2 ways—namely, via emission of an α-particle with an energy of 5.87 MeV to ^{207}Bi or via an electron capture (EC) process to

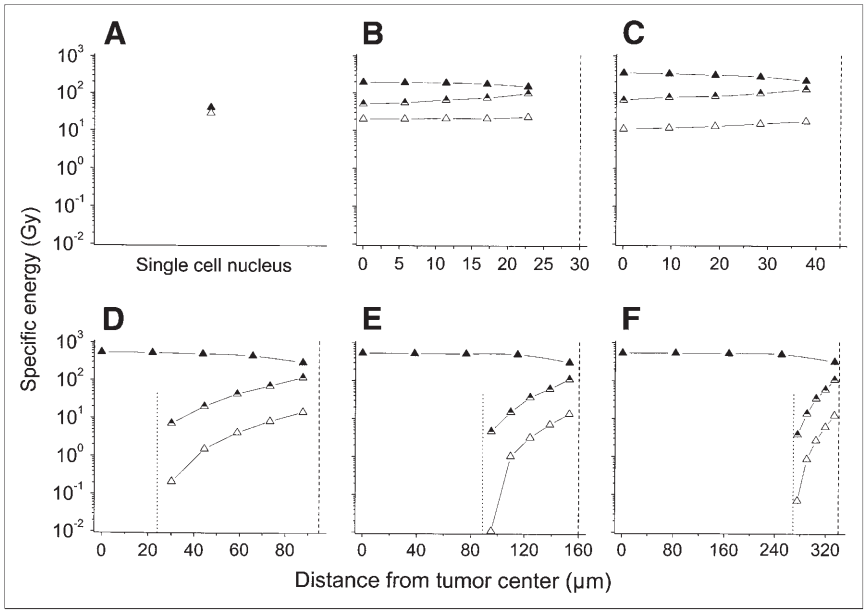

FIGURE 4. Specific energy to single cell nucleus and to cell nuclei in tumors as function of distance from tumor center. Injected activity was 400 kBq. Size of tumors was determined by SEM at time of treatment—that is, at 1, 3, 4, 5, and 7 wk after cell inoculation. For a single cell (A), calculations were performed for 2 cases: ^{211}At-MX35 F(ab′)$_2$ distributed at all antigenic sites on cell surface (▲) and ^{211}At-Rituximab F(ab′)$_2$ freely circulating in abdominal fluid surrounding the cell—that is, no specific binding (△). For tumors (B–F), calculations were performed for 3 cases: ^{211}At-MX35 F(ab′)$_2$ homogeneously distributed at all antigenic sites on all cells throughout the whole tumor (▲), ^{211}At-MX35 F(ab′)$_2$ distributed only on surface of tumor (▲), and ^{211}At-Rituximab F(ab′)$_2$ freely circulating in abdominal fluid surrounding the tumor—that is, no specific binding (△). Dashed line (- - -) represents surface of tumor and dotted line (· · ·) represents largest depth that those α-particles with the longest path length, s_{max}, emitted from surface of the tumor, reached.

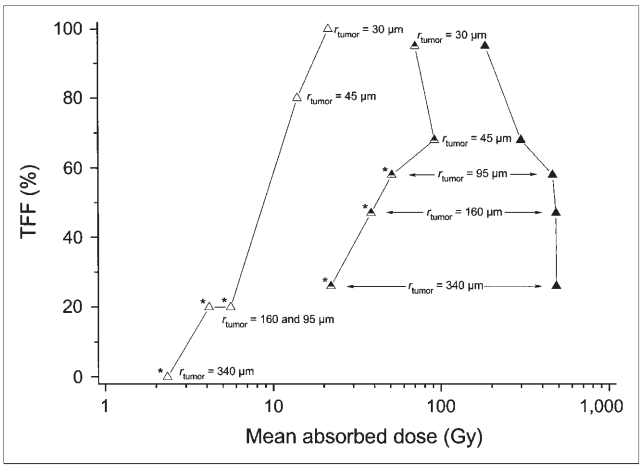

FIGURE 5. TFF as function of mean absorbed dose to differently sized tumors for unbound ^{211}At-Rituximab F(ab′)$_2$ (△), ^{211}At-MX35 F(ab′)$_2$ bound only to surface of tumors (▲), and ^{211}At-MX35 F(ab′)$_2$ bound to all antigenic sites throughout whole tumor (▲). Injected activity was 400 kBq. Tumor radii of 30, 45, 95, 160, and 340 μm correspond to largest tumor found at 1, 3, 4, 5, and 7 wk after cell inoculation, respectively. Asterisk on some symbols indicates presence of unirradiated cell nuclei (receiving zero specific energy) in core of tumor, because $r_{tumor} > s_{max}$. For these tumors, fraction of unirradiated cell nuclei was 0.016, 0.172, and 0.495 for r_{tumor} = 95, 160, and 340 μm, respectively.

^{211}Po. ^{207}Bi decays via EC with a half-life of 31.55 y to ^{207}Pb (stable), whereas ^{211}Po decays with a half-life of 0.52 s to ^{207}Pb via emission of an α-particle of 7.45 MeV. As the decay to ^{207}Bi or ^{211}Po occurs, the chemical properties will change and the binding to the mAb will probably be broken (*29*). In the case of ^{211}Po, this implies that the α-particle will be emitted from a location other than that of the mAb, with the distance away being determined by diffusion. In the case in which the mAbs are assumed to be distributed homogeneously throughout the whole tumor, this will probably have a negligible effect on the specific energy to tumor cell nuclei. However, in the single-cell case and in the case in which the mAbs are assumed to be situated only on the surface of the tumor, the escape of the ^{211}Po atom from the mAb could alter the irradiation geometry and, with it, the specific energy. This effect can reduce the number of cell nuclei events (and, hence, the specific energy) by a factor of ~2 (*29*).

Calculation of the specific energy originating from binding of the mAbs to the antigenic sites on the tumor cells were performed for 2 hypothetic extreme conditions: First, all tumor cells and antigenic sites in a tumor were available to the mAbs, and free diffusion of the mAbs into the tumor tissue occurred. This situation was assumed for the purpose of estimating the maximum attainable specific energy to tumor cell nuclei. Second, no diffusion occurred into the tumors, resulting in an ^{211}At-mAb distribution only on the surface of the tumor. This means that the radiation will not reach the core of the tumor when $r_{tumor} > s_{max}$.

The mean absorbed dose was generally high (Fig. 5), especially when an RBE of 3–5 is considered. Even for the nonspecific mAb, a high mean absorbed dose (~14–21 Gy) was obtained for $r_{tumor} \leq 45$ μm (Fig. 5), indicating a high probability for sterilization. For the specific mAb, the mean absorbed dose was even higher (>22 Gy) for all tumor sizes, even if only tumor surface-bound activity was considered. For r_{tumor} equal to 95, 160, or 340 μm, the specific energy equaled zero at a distance from the tumor surface greater than s_{max}, when the ^{211}At-mAbs were assumed to be located only on the surface of the tumors or circulating in the fluid surrounding them (Fig. 4).

The outcome—that is, the TFF—was plotted against the mean absorbed dose to the largest tumor for each study group (Fig. 5). The largest tumors are most difficult to eradicate because of the large number of cells present in these tumors. Therefore, the mean absorbed dose to these tumors should be decisive for the outcome. The stated maximum sizes are based on random samples in a control group. Deviations from these values will certainly affect the outcome in individuals and, consequently, the relation between TFF and mean absorbed dose. We estimate that the shown maximum sizes could vary by ±10% at most, compared with the true value, because of (a) individual variations, (b) ellipsoid tumors being approximated as spheres, and (c) error in size estimation when using the ruler in the electron microscope. The reduced TFF for the specific mAb already at a r_{tumor} = 45 μm could be caused by some individuals having larger tumors. Correspondingly, in the case of r_{tumor} = 340 μm, the tumor size in individual animals may have been smaller, explaining the fact that some animals have been cured. But in this case, it seems more probable that penetrating mAbs contributed to the irradiation, increasing the specific energy, especially to the core of the tumor. The low TFF of 25% for r_{tumor} = 340 μm indicates that penetration is restricted. The nonspecific mAb gives a more pronounced decrease in TFF when $r_{tumor} > s_{max}$. This is in correspondence with a drastic decrease in mean absorbed dose and no irradiation of the tumor core.

Because of a difference in the carbon−halogen bond strength between ^{211}At- and ^{125}I-MX35 F(ab′)$_2$, 205 and 260 kJ/mol, respectively, somewhat more ^{211}At than ^{125}I will be released in vivo. This explains the difference in organ content between the 2 nuclides.

CONCLUSION

Treatment with ^{211}At-mAb resulted in a TFF of 95%−100% when $r_{tumor} \leq 30$ μm and the specific energy was >20 Gy to cell nuclei in the tumor. The TFF was drastically decreased (TFF ≤ 20%) for the nonspecific mAb when $r_{tumor} > s_{max}$, resulting in a low mean absorbed dose (<6 Gy) and 0 Gy to the tumor core. The specific mAb gave for these tumor sizes a significantly better TFF, explained by a higher mean absorbed dose (>22 Gy) from

mAb bound to the tumor surface, and probably some contribution from penetrating mAbs. The rather low TFF of ~25% for the largest tumor size using the specific mAb, however, is not consistent with a major contribution from penetrating mAbs.

ACKNOWLEDGMENTS

This work was conducted at The Sahlgrenska Academy at Göteborg University and was supported by grants from the Swedish Cancer Foundation (no. 3548) and the King Gustaf V Jubilee Clinic Research Foundation in Göteborg, Sweden. We thank Dr. Chaitanya R. Divgi, Director of Targeted Radiotherapy at the MSKCC, for making the mAb MX35 $F(ab')_2$ available. The electron microscopy specimen preparation of Yvonne Josefsson and Gunnel Bokhede is acknowledged. Electron microscopy equipment was funded by the Lundberg Research Foundation.

REFERENCES

1. Berkenbilt A, Cannistra SA. Advances in the management of epithelial ovarian cancer. *J Reprod Med.* 2005;50:426–438.
2. Agarawal R, Kaye SB. Ovarian cancer: strategies for overcoming resistance to chemotherapy. *Nat Rev Cancer.* 2003;3:502–506.
3. Goldenberg DM. Targeted therapy of cancer with radiolabeled antibodies. *J Nucl Med.* 2002;43:693–713.
4. McQuarrie S, Mercer J, Syme A, Suresh M, Miller G. Preliminary results of nanopharmaceuticals used in the radioimmunotherapy of ovarian cancer. *J Pharm Pharm Sci.* 2005;7:29–34.
5. Janssen ML, Pels W, Massuger LF, et al. Intraperitoneal radioimmunotherapy in an ovarian carcinoma mouse model: effect of the radionuclide. *Int J Gynecol Cancer.* 2003;13:607–613.
6. Borchardt PE, Quadri SM, Freedman RS, Vriesendorp HM. Intraperitoneal radioimmunotherapy with human monoclonal IGM in nude mice with peritoneal carcinomatosis. *Cancer Biother Radiopharm.* 2000;15:53–64.
7. Grana C, Bartolomei M, Handkiewicz D, et al. Radioimmunotherapy in advanced ovarian cancer: Is there a role for pre-targeting with ^{90}Y-biotin? *Gynecol Oncol.* 2004;93:691–698.
8. Meredith RF, Alvarez RD, Partridge EE, et al. Intraperitoneal radioimmunochemotherapy of ovarian cancer: a phase I study. *Cancer Biother Radiopharm.* 2001;16:305–315.
9. Mahe MA, Fumoleau P, Fabbro M, et al. A phase II study of intraperitoneal radioimmunotherapy with iodine-131-labeled monoclonal antibody OC-125 in patients with residual ovarian carcinoma. *Clin Cancer Res.* 1999;5: 3249–3252.
10. Epenetos AA, Hird V, Lambert H, Mason P, Coulter C. Long term survival of patients with advanced ovarian cancer treated with intraperitoneal radioimmunotherapy. *Int J Gynecol Cancer.* 2000;10:44–46.
11. Alvarez RD, Partridge EE, Khazaeli MB, et al. Intraperitoneal radioimmunotherapy of ovarian cancer with ^{177}Lu-CC49: a phase I/II study. *Gynecol Oncol.* 1997;65:94–101.
12. Alvarez RD, Huh WK, Khazaeli MB, et al. A phase I study of combined modality ^{90}yttrium-CC49 intraperitoneal radioimmunotherapy for ovarian cancer. *Clin Cancer Res.* 2002;8:2806–2811.
13. Stewart JSW, Hird V, Snook D, et al. Intraperitoneal yttrium-90-labeled monoclonal antibody in ovarian cancer. *J Clin Oncol.* 1990;8:1941–1950.
14. Seiden M, Benigno BB. The SMART study investor group, Southeastern Gynecological Oncology: a pivotal phase III trial to evaluate the efficacy and safety of adjuvant treatment with R1549 (yttrium-90-labeled HMFG1 murine monoclonal antibody) in epithelial ovarian cancer (EOC) [abstract]. *Proc Am Soc Clin Oncol.* 2004; abstract 5008.
15. Andersson H, Elgqvist J, Horvath G, et al. Astatine-211-labeled antibodies for treatment of disseminated ovarian cancer: an overview of results in an ovarian tumor model. *Clin Cancer Res.* 2003;9:3914–3921.
16. Bäck T, Andersson H, Divgi CR, et al. ^{211}At-radioimmunotherapy of subcutaneous human ovarian cancer xenografts: evaluation of RBE of an alpha emitter in vivo. *J Nucl Med.* 2005;46:2061–2067.
17. Andersson H, Lindegren S, Bäck T, Jacobsson L, Leser G, Horvath G. Radioimmunotherapy of nude mice with intraperitoneally growing ovarian cancer xenograft utilizing ^{211}At-labelled monoclonal antibody MOv18. *Anticancer Res.* 2000;20:459–462.
18. Andersson H, Lindegren S, Bäck T, Jacobsson L, Leser G, Horvath G. The curative and palliative potential of the monoclonal antibody MOv18 labelled with ^{211}At in nude mice with intraperitoneally growing ovarian cancer xenografts: a long term study. *Acta Oncol.* 2000;39:741–745.
19. Andersson H, Palm S, Lindegren S, et al. Comparison of the therapeutic efficacy of ^{211}At- and ^{131}I-labelled monoclonal antibody MOv18 in nude mice with intraperitoneal growth of human ovarian carcinoma. *Anticancer Res.* 2001;21: 409–412.
20. Elgqvist J, Andersson H, Bäck T, et al. Therapeutic efficacy and tumor dose estimations in radioimmunotherapy of intraperitoneally growing OVCAR-3 cells in nude mice with the ^{211}At-labeled monoclonal antibody MX35. *J Nucl Med.* 2005;46:1907–1915.
21. Lindegren S, Bäck T, Jensen HJ. Dry-distillation of astatine-211 from irradiated bismuth targets: a time-saving procedure with high recovery yields. *Appl Radiat Isot.* 2001;55:157–160.
22. Welshinger M, Yin BWT, Lloyd KO. Initial immunochemical characterization of MX35 ovarian cancer antigen. *Gynecol Oncol.* 1997;67:188–192.
23. Rubin SC, Kostakoglu L, Divgi C, et al. Biodistribution and intraoperative evaluation of radiolabeled monoclonal antibody MX35 in patients with epithelial ovarian cancer. *Gynecol Oncol.* 1993;51:61–66.
24. Reff ME, Carner K, Chambers KS, et al. Depletion of B cells in vivo by a chimeric mouse human monoclonal antibody to CD20. *Blood.* 1994;83:435–445.
25. Lindegren S, Andersson H, Bäck T, Jacobsson L, Karlsson B, Skarnemark G. High-efficiency astatination of antibodies using N-iodosuccinimide as the oxidizing agent in labeling of N-succinimidyl 3-(trimethylstannyl)benzoate. *Nucl Med Biol.* 2001;28:33–39.
26. Hamilton TC, Young RC, McKoy WM, et al. Characterization of a human ovarian carcinoma cell line (NIH:OVCAR-3) with androgen and estrogen receptors. *Cancer Res.* 1983;43:5379–5389.
27. Lindmo T, Boven E, Cuttitta F, Fedorko J, Bunn PA. Determination of the immunoreactive fraction of radiolabeled monoclonal antibodies by linear extrapolation to binding at infinite antigen excess. *J Immunol Methods.* 1984;72: 77–89.
28. Friedman PL, Ellisman MH. Enhanced visualization of peripheral nerve and sensory receptors in the scanning electron microscope using cryofracture and osmium-thiocarbohydrazide-osmium impregnation. *J Neurocytol.* 1981;10: 111–131.
29. Palm S, Humm JL, Rundqvist R, Jacobsson L. Microdosimetry of astatine-211 single-cell irradiation: role of daughter polonium-211 diffusion. *Med Phys.* 2004; 31:218–225.
30. ICRU. *Stopping Powers and Ranges for Protons and Alpha Particles.* Publication 49. Bethesda, MD: International Commission on Radiation Units and Measurements; 1993.
31. Elgqvist J, Bernhardt P, Hultborn R, et al. Myelotoxicity and RBE of ^{211}At-conjugated mAbs compared to ^{99m}Tc-conjugated mAbs and ^{60}Co irradiation in nude mice. *J Nucl Med.* 2005;46:464–471.
32. Horak E, Hartmann F, Garmestani K, et al. Radioimmunotherapy targeting of HER2/neu oncoprotein on ovarian tumor using lead-212-DOTA-AE1. *J Nucl Med.* 1997;38:1944–1950.

JNM The Journal of NUCLEAR MEDICINE

α-Radioimmunotherapy of Intraperitoneally Growing OVCAR-3 Tumors of Variable Dimensions: Outcome Related to Measured Tumor Size and Mean Absorbed Dose

Jörgen Elgqvist, Håkan Andersson, Tom Bäck, Ingela Claesson, Ragnar Hultborn, Holger Jensen, Bengt R. Johansson, Sture Lindegren, Marita Olsson, Stig Palm, Elisabet Warnhammar and Lars Jacobsson

J Nucl Med. 2006;47:1342-1350.

The Journal of Nuclear Medicine is published monthly.
SNMMI | Society of Nuclear Medicine and Molecular Imaging
1850 Samuel Morse Drive, Reston, VA 20190.
(Print ISSN: 0161-5505, Online ISSN: 2159-662X)

SNMMI SOCIETY OF NUCLEAR MEDICINE AND MOLECULAR IMAGING